AIAA SciTech Forum
11–15 & 19–21 January 2021, VIRTUAL EVENT
AIAA Scitech 2021 Forum

10.2514/6.2021-1975

Ion-Induced Electron Emission from Surfaces Bombarded by an EMIM-BF_4 Electrospray Plume

Matthew R. Klosterman,[1] Joshua L. Rovey,[2] and Deborah Levin[3]
University of Illinois Urbana-Champaign, Urbana, IL, 61801, USA

Experiments have been conducted at the University of Illinois Urbana Champaign Electric Propulsion Laboratory to study the ion-induced electron emission behavior of surfaces being bombarded by cations and anions in an [EMIM][BF_4] electrospray plume. The surfaces tested include 6061 aluminum, carbon graphite, 316 stainless steel, and grade 5 titanium. Operation in cation mode resulted in yields from 0.5-2.5 emitted electrons per incident ion for emitter voltages of 2.2-3.0 kV. Additionally, the energy of electrons emitted from surfaces bombarded by cations increases linearly with emitter voltage and ranges from 80-165 eV depending on the surface material. A hysteresis effect is identified in the suppression of electron emission during cation bombardment and strongly depends on the target material and emitter voltage. Further, results indicate that 85-95% of the current from electron emission in cation mode travels upstream and is collected by the emitter. Operation in anion mode resulted in much lower yields of < 0.2 emitted electrons per incident ion over the range of 2.2-3.0 kV emitter voltages. However, evidence is presented showing that anion yields can increase to > 1 when surfaces are negatively biased.

I. Nomenclature

I_{Ion}	=	ion current, nA
I_{Total}	=	total current, nA
I_{IIEE}	=	ion induced electron emission current, nA
KE	=	kinetic energy, J
$m_{monomer}$	=	mass of monomer ion, amu
m_{dimer}	=	mass of dimer ion, amu
V_0	=	emitter voltage or extraction potential, kV
Y_{IIEE}	=	electron emission yield, electrons/ion

II. Introduction

Electrospray propulsion has quickly become a popular candidate for small satellite propulsion. In electrospray thrusters, ions from room-temperature ionic liquids (IL) are electrostatically accelerated to high velocities (>10,000 m/s) to provide thrust. Recent development has focused on porous-glass electrospray thrusters [1–4], which passively feed the IL through a porous glass substrate with machined tips towards a charged extraction grid. These thrusters typically emit in a pure-ion regime in which the plume mainly consists of single ions (monomers) or ions attached to a neutral pair (dimers), resulting in very high specific impulse (>1500 s).

A significant challenge in the development of electrospray thrusters is the effect of the facility on experimental results and the corresponding challenge of correcting or modifying ground-based measurements to predict in-space behavior. Recent literature identifies anomalous thruster test results that may be due to plume-facility interactions. Testing of electrically isolated thruster systems, similar to a spacecraft configuration, has shown anomalous spacecraft charge loss [2,5] which may be caused by plume ions returning to the charged spacecraft and causing ion-induced electron emission (IIEE). The University of Southampton reported possible IIEE interference in time-of-flight and

[1] Graduate Research Assistant, Department of Aerospace Engineering, mkloste2@illinois.edu
[2] Associate Professor, Department of Aerospace Engineering, and AIAA Associate Fellow, rovey@illinois.edu
[3] Professor, Department of Aerospace Engineering, and AIAA Fellow, deblevin@illinois.edu

current collection measurements [1,2,6] and experiments at MIT suggest IIEE from a faraday cup explains anomalous retarding potential analyzer (RPA) traces of cation energy distribution [7].

The following sections describe experiments that measure the IIEE yields from common thruster, facility, and spacecraft materials bombarded by an electrospray plume. A single externally wetted tungsten needle emitter is used to create an electrospray plume of [Emim][BF_4] IL that is directed onto target surfaces. Results for the first time show the effect of emitter voltage and operating polarity on the IIEE yield and emitted electron energy, and also show evidence of hysteresis in the IIEE. The experimental setup is described in the next section followed by the experimental results, analysis, and conclusions.

III. Experimental Setup

A. Facility Description

The electrospray experiments are performed in a 24" dia. x 27" vacuum chamber equipped with one CTI Cryo-Torr 8 cryopump powered by a Brooks 9600 helium compressor and roughed by a dry mechanical pump. The chamber has a base pressure of $4x10^{-6}$ Torr and all experiments are performed at an operating pressure below $3x10^{-5}$ Torr. Inside the chamber, a Newmark Systems RM-3 rotary stage is mounted on an optical breadboard plate with a mount for an electrospray emitter/extractor assembly.

B. Emitter Properties

A single etched 0.5 mm dia. tungsten wire externally wetted emitter is used as the electrospray source in all experiments. This type of emitter is well characterized in the literature [8,9] and typically emits in the pure-ion regime similar to a porous glass electrospray thruster. The emitter is electrochemically etched following the procedure in [8], and further details are given here. The tip is dipped in a 2N NaOH solution at 50 V until there is a smooth, concave curvature from the wire to a rounded point. A 0.25 mm dia. tungsten wire is spot welded orthogonally ~3 mm from the tip to provide an IL reservoir. The tip/reservoir assembly is submerged for 45 seconds in a 1N NaOH solution saturated with $K_3Fe(CN)_6$ at 90-95°C to roughen the surface of the emitter for better fluid transport to the tip. The resulting emitter has a tip radius of curvature of ~32 μm and is shown in Figure 1a. The emitter with the crossbar attached, mounted in its copper holder is shown in Figure 1b.

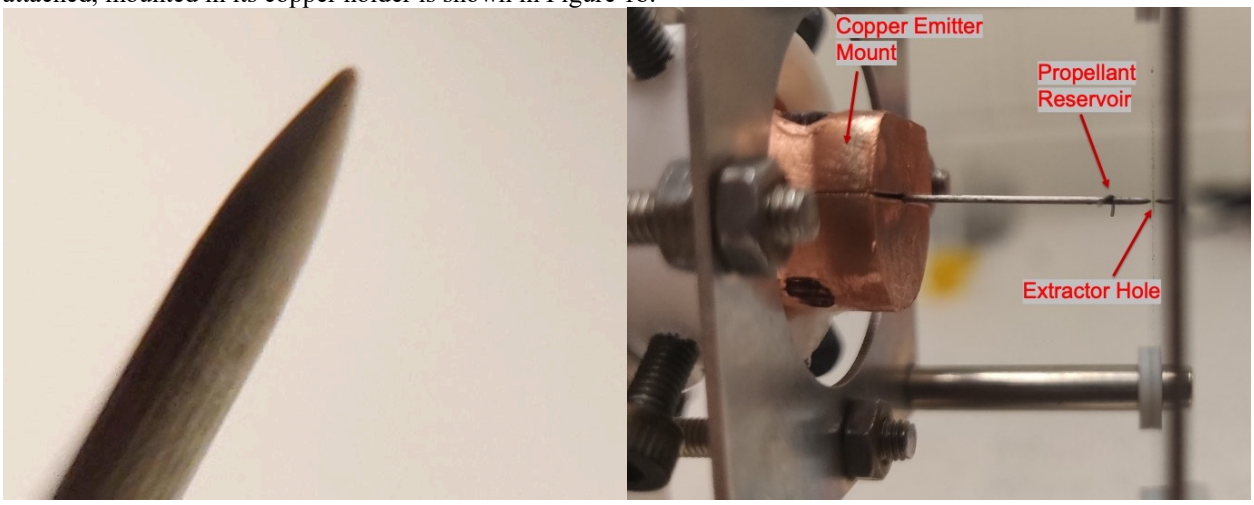

(a) (b)

Figure 1: Tungsten wire externally wetted electrospray emitter (a) up close and (b) mounted in front of the 1.4 mm hole in the extractor grid

Before testing, the emitter is ultrasonically cleaned in distilled water for 10 minutes, then in ethanol for 10 minutes to remove the water. After drying with compressed air a heat gun is used to heat the tip/reservoir assembly for 1 minute. A syringe is then used to drag a drop of [EMIM][BF_4] over the tip and back to the reservoir while ensuring that the emitter is wetted on all sides. The emitter is mounted on a copper block that serves as an electrical lead and heat sink. A 1 mm thick stainless steel extractor plate has a 1.4 mm diameter hole centered on the emitter tip and is located 0.1 mm downstream of the emitter tip. The entire assembly is mounted in the vacuum facility as described above and the chamber is pumped down to operating pressure.

C. Electrical and Diagnostics Setup

The emitter and extractor are each connected to a Matsusada AMS-5B6 high voltage amplifier. The extractor amplifier is grounded for all experiments here and the emitter is operated in a 1 Hz square-wave AC mode with a peak-to-peak value of 2x the emitter bias voltage. A custom high-voltage current monitor is connected between each amplifier and the emitter/extractor. This current monitor consists of a TI AMC1311 isolation amplifier that reads the voltage drop across a 1 MΩ shunt resistor on the high voltage side and outputs a differential signal at ground with a gain of one. Because the isolation amplifier is a single-polarity device, a diode is used to direct the current towards different devices for positive and negative emission modes.

A Kimball Physics faraday cup with retarding potential analyzer grids is mounted to one side of the emitter. Current to the faraday cup is measured by a Keithley 6514 electrometer and the retarding grid is biased using an SRS PS350 high voltage power supply. An NI USB-6211 data acquisition unit measures analog signals from all instruments and controls the high-voltage amplifiers via analog output. Data is recorded on a PC using the NI DAQExpress software. The faraday cup is used to measure the plume current density distribution and plume ion energy distribution, and results are compared with literature data for other emitters to verify similar or typical operation.

For plume-surface interactions experiments, the emitter is aimed at a 6”x6” plate of the material of interest. The target plate is mounted 8 cm from the extractor as illustrated in Figure 2a resulting in a 43° capture angle of the plume – far greater than the measured 17° divergence angle – such that the entire plume impinges on the target. Figure 2b illustrates the electrical setup of the IIEE experiments. The emitter is operated in AC mode at 1 Hz and the currents to the emitter and extractor are measured as described above. Electron emission from the target surface is suppressed by applying a positive bias to the target using an SRS PS350 power supply. Another custom current monitor (identical to those described above) is placed between the power supply and the target plate to measure the total current to the plate, which will be the combined currents of ions going to the plate and electrons leaving the plate.

It is important to the interpretation of the data in these experiments to keep straight the effect of each charge species on the measured target plate current. In positive emission mode, cations arriving at the surface and electrons leaving the surface both yield a positive current. In this case electron emission would cause a higher positive current than would be measured with no electron emission. In negative emission mode, anions arriving at the surface yield a negative current while electrons leaving the surface are still a positive current. In this case electron emission would cause a lower magnitude negative current (less negative) than would be measured with no electron emission.

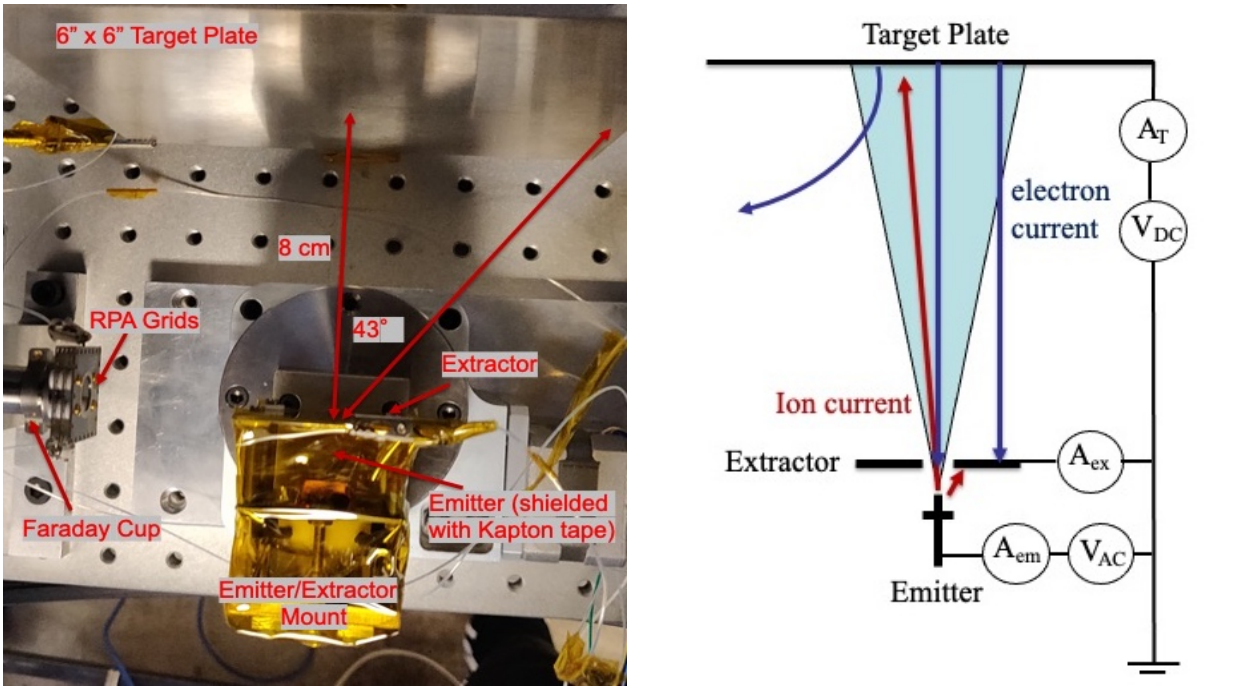

(a) (b)

Figure 2: Ion-induced electron emission experimental setup. (a) Image of the emitter and target plate setup in the facility. (b) Electrical schematic of the IIEE experimental setup.

IV. Results

This section describes the results obtained from the experimental setup described above. The performance of the emitter is quantified by emission current, plume current distribution, and plume energy distribution. The measured current data are presented and used to calculate IIEE yields and emitted electron energy. Evidence of hysteresis in the current measurements is identified, as well as anion induced electron emission from negatively biased surfaces.

A. Emitter Operation

The performance of the emitter is compared in Figure 3 to similar emitters in the literature and in use at Air Force Research Lab Kirtland for [EMIM][BF_4] electrosprays.

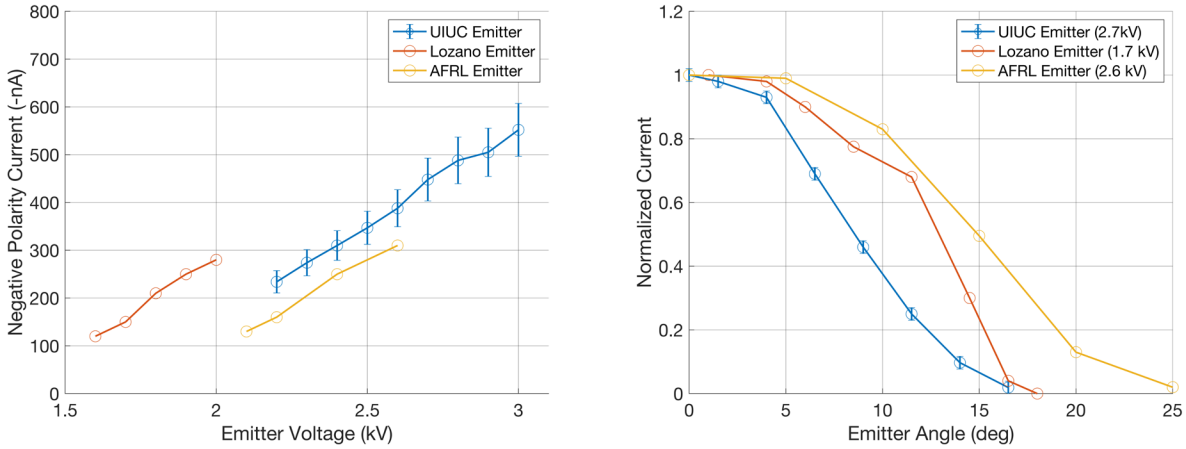

(a) (b)

Figure 3: Emitter performance compared to [8] **and an emitter tested by the author at AFRL Kirtland. (a) Emitter current at different emitter voltages in anion (negative) mode. (b) Plume current angular distribution.**

Figure 3a illustrates the measured emitter current in the negative polarity mode which linearly increases in magnitude from 200-600 nA for emitter voltages between 2.2-3.0 kV. The starting voltage varies between 1.6 kV for the emitter characterized in [8] and 2.2 kV for the emitter used in these experiments, a difference likely due to the emitters having tip radii of ~20 μm and ~32 μm, respectively. An increase in emitter tip curvature corresponds to an increase in starting voltage as pointed out in [8]. Figure 3b illustrates the current density distribution of the electrospray plume and the beam half-cone angle of the emitter used in these experiments is 17°. The measurements of each emitter are normalized by the centerline current density and, although the half-cone angles vary between 17-25°, each emitter follows the same normal distribution trend.

An RPA trace at the centerline of the plume and ~3 cm from the emitter is shown in Figure 4a. This trace compares well with data in the literature for [EMIM][BF_4] plumes from both tungsten wire emitters and porous glass electrospray thrusters [1,7]. In an ideal electrospray plume all ions would be fully accelerated by the extraction potential and the normalized current would drop from 1 to 0 when the retarding potential reaches the extraction potential – at a normalized RPA voltage of 1. Instead, what is illustrated in Figure 4a is that cation and anion dimers in the plume fragment into one ion monomer and one neutral pair. If this fragmentation occurs downstream of the extractor, the ion monomer will have a kinetic energy proportional to its mass divided by the dimer mass as calculated in Equation 1. This energy level is marked in Figure 4 by the vertical blue and red dashed lines for cations ($0.360V_0$) and anions ($0.305V_0$), respectively.

$$KE = \frac{m_{monomer}}{m_{dimer}} V_0 \tag{1}$$

If fragmentation occurs in the acceleration region between the emitter and extractor, the ion monomer is still accelerated by the electric field and will have a kinetic energy somewhere between the zero-field fragment energy and the total extraction energy. The steady drop in current denoted “accel-region fragmentation” consists of ions that fragmented at different locations in the acceleration region and suggests that there is an equal probability of fragmentation at all locations between the emitter and extractor. Figure 4b illustrates the derivative of the normalized

current in Figure 4a with respect to energy. This calculation yields an approximate energy distribution of the plume with peaks at the "zero-field fragmentation" energy and at the full acceleration energy. The anomalous peak and drop in anion current before the zero-field fragmentation energy in Figure 4a is explained as an effect of electron emission from the negatively biased RPA grids (note that we see IIEE due to anion bombardment significantly increases when a surface is biased negatively) and is likely not a measure of anion current. Each of the effects identified in the RPA data is also observed in the literature [1,7].

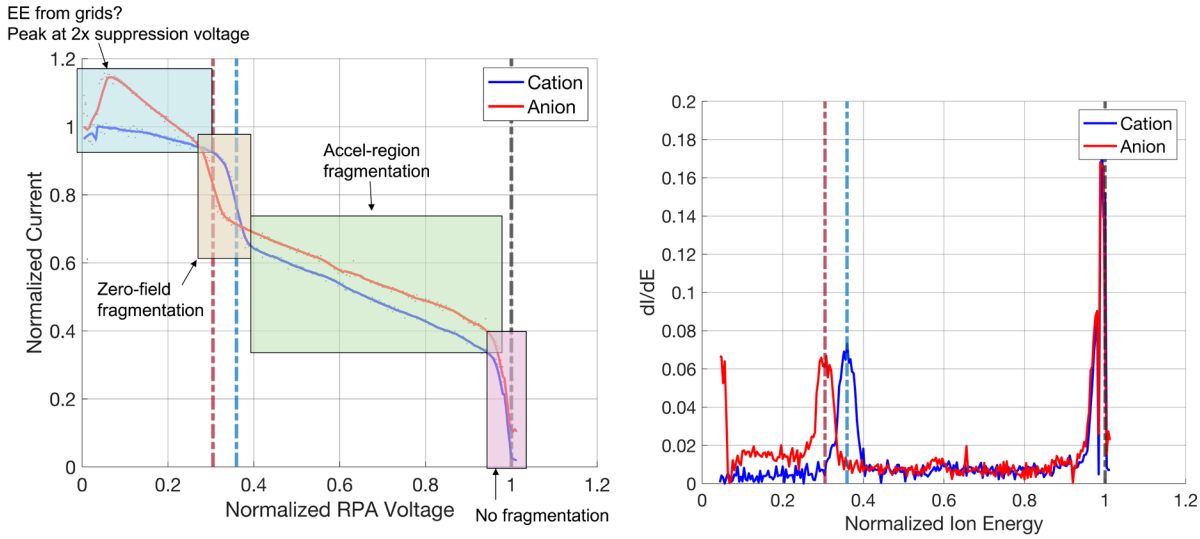

(a) (b)

Figure 4: RPA data from the centerline of the plume. (a) Normalized collected current vs. RPA voltage (normalized by emitter voltage). (b) Derivative of normalized current vs. ion energy yields the energy distribution.

While this emitter has not been tested with more advanced diagnostics such as time-of-flight mass spectrometry, we assume based on these favorable comparisons with literature data that the composition of the plume is comparable to other tungsten wire emitters and porous glass electrospray thrusters, which have plume composition of 40-50% monomers and 50-60% dimers [4,8].

B. Positively Biased Target Plate Studies

Figure 5 illustrates the change in measured currents to the 6061 aluminum, carbon graphite, 316 stainless steel, and grade 5 titanium targets as the bias on the plate is increased for an emitter voltage of 2.6 kV. In each plot, the anion and cation currents measured at the emitter, extractor, and target plates are shown.

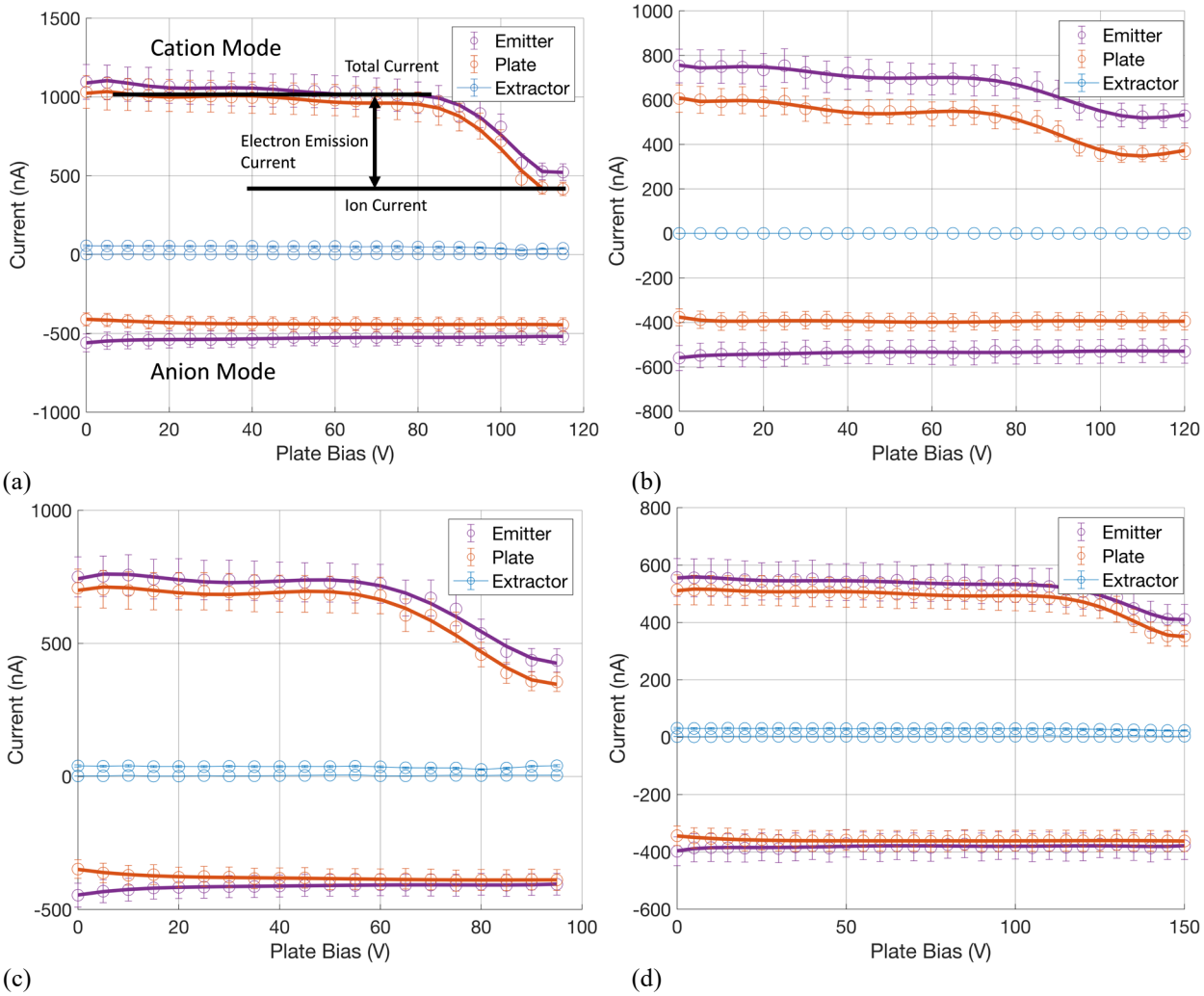

Figure 5: Effect of target bias potential on emitter, extractor, and target currents for (a) 6061 aluminum, (b) carbon graphite, (c) 316 stainless steel, and (d) grade 5 titanium target materials at an emitter voltage of 2.6 kV.

In cation mode (positive current) for the aluminum plate at a plate bias of 0 V the target current is approximately 1000 nA. As the plate bias increases the target current remains approximately constant until a bias voltage of approximately 80 V, at which point the current decreases. At about 110 V the cation target current plateaus at a reduced value of just below 500 nA. This change in target current due to changing target bias potential is due to IIEE suppression, and we define the difference between the target current at 0 V (labeled "total current") and 110 V (labeled "ion current") as the IIEE current for an aluminum target at an emitter voltage of 2.6 kV. In cation mode the emitter current also changes with target bias voltage even though the emitter voltage is constant. Specifically, the emitter current trends track closely with the target plate current. Note that negative charge collection at the emitter would give rise to an increase in measured positive current at the emitter. The close agreement between target and emitter current is attributed to emitted electrons from the target travelling upstream and being collected by the emitter. In anion mode (negative current) for the aluminum plate at a bias of 0 V the target current is just below 500 nA and increases by only approximately 35 nA as the plate bias is increased to 115 V. This 7% change in current is within the error of the measurement so it cannot be determined whether it is from the suppression of IIEE. Similar target and emitter current trends are measured for all target materials tested, as shown in Figure 5. No appreciable change in extractor current with target bias is measured, and in all cases the extractor current is less than 10% of the emitter current.

Figure 5 shows the change in measured currents as the positive bias on the target plate increases from 0 V to a potential large enough to suppress electron emission (e.g., 110 V for aluminum in Figure 5a). However, the results

are different when the target plate bias is then decreased and returned to 0 V ground potential. Figure 6a illustrates this hysteresis for aluminum.

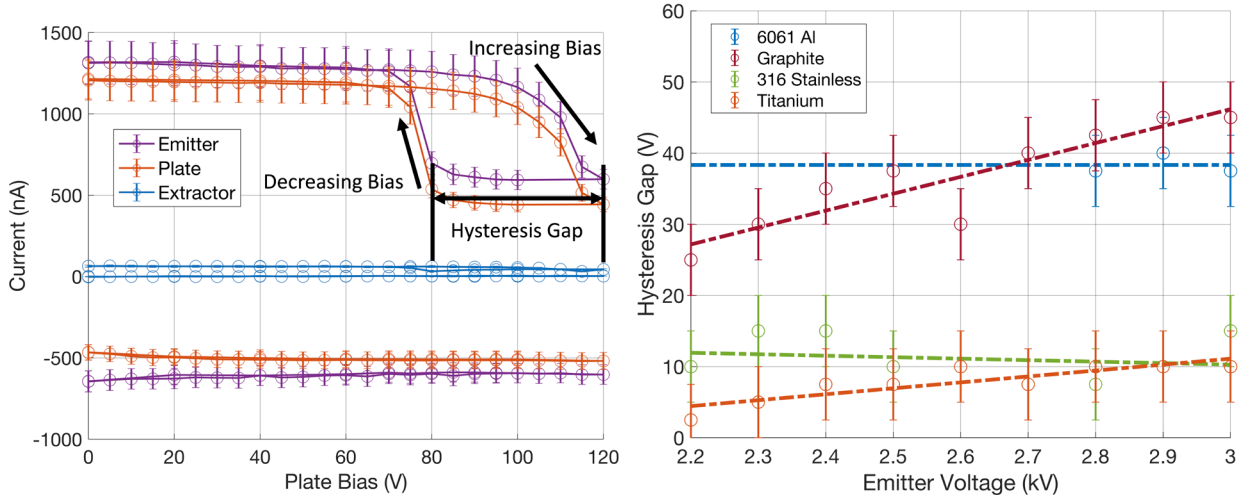

(a) (b)

Figure 6: (a) Example of hysteresis loop in measured target plate and emitter current as plate bias voltage is increased and then decreased at 2.8 kV emitter voltage for an aluminum target plate. (b) Measured hysteresis gap (difference in the required plate voltage to suppress electron emission when increasing or decreasing the plate bias voltage), a function of material and emitter voltage.

When the electron emission has been fully suppressed by increasing the target plate bias voltage, the target bias voltage is then decreased back to ground and the voltage at which electron emission restarts is lower than the point where it is initially suppressed. This behavior is a hysteresis loop in the measured current, and we define the hysteresis gap width as the difference between the voltage required to suppress electron emission when increasing the voltage and the voltage at which electron emission restarts when decreasing the voltage. This hysteresis gap can be as large as 45 V depending on the target material. For aluminum, Figure 6a illustrates the current measured at the target plate and emitter in cation mode along the top path decreases at approximately 90 V and plateaus at 120 V. As the bias on the plate is then decreased from 120 V, the current measured at the target plate and emitter follows the bottom path, and increases at approximately 85 V and reaches the original current at 70 V. The difference in voltage at the suppression and restarting of electron emission, denoted the hysteresis gap in Figure 6a, is plotted for each material in Figure 6b. This effect is very prominent (25-45 V) in the aluminum and carbon graphite, but less significant (5-15 V) in the stainless steel and titanium. The carbon graphite results show the strongest dependence on emitter voltage, increasing from 25-45 V over the range of 2.2-3.0 kV emitter voltages. The metals are not as strongly dependent on the emitter voltage in this range, with titanium increasing by only 7.5 V and aluminum and stainless steel remaining approximately constant.

C. Negatively Biased Grid and Target Plate Studies

Standard, or certainly common, practice for current collection in electrospray diagnostics is to mount a metallic mesh grid directly in front of the charge collecting surface and bias the grid negative to suppress electron emission from the grounded collector. We investigate this type of setup by placing a 304 stainless steel grid with a 73% open area fraction ~ 3 mm in front of the collecting surface and include an additional current monitor on the suppression grid. The current to the suppression grid as it is negatively biased is illustrated in Figure 7a. We compare this grid-bias approach with the previously described setup (no grid, directly biasing the target plate) with the target plate directly biased negatively in Figure 7b. Results suggest that IIEE occurs from a negatively biased surface in both cation and anion modes, and can mask the ion current measurement. Specifically, electron current from the grid (caused by IIEE) goes to either the target plate or back to the emitter/extractor, and it becomes more difficult to determine exactly which currents are being measured.

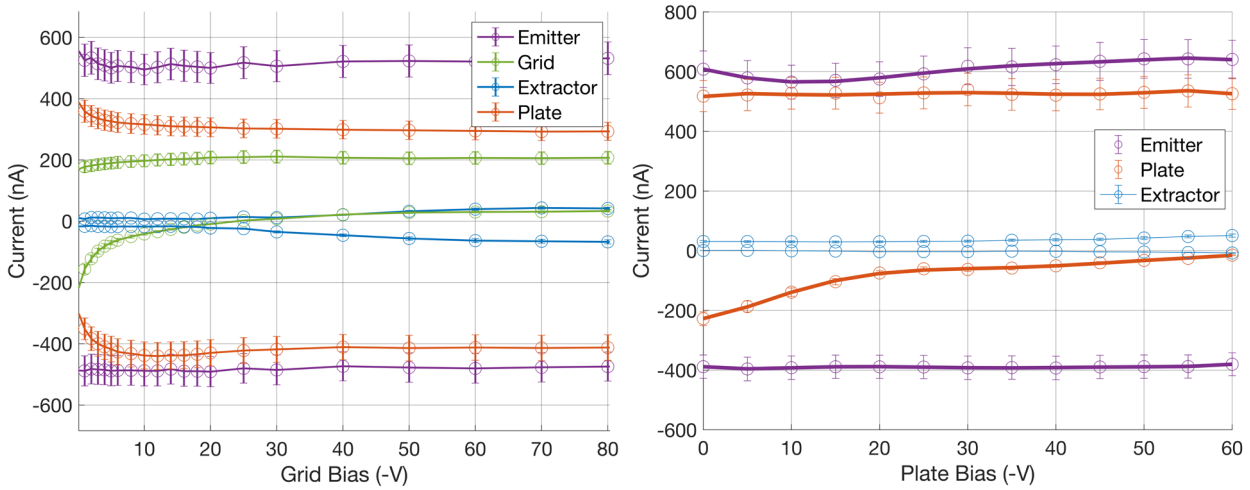

(a) (b)

Figure 7: (a) Emitter, grid, extractor, and target plate currents in anion and cation modes as the electron suppression grid is biased negatively. (b) Effect of a negative bias voltage on measured currents for a 316 stainless steel plate with no electron suppression grid.

Figure 7a illustrates the change in measured currents for an aluminum target plate at 2.7 kV emitter voltage as the bias on the suppression grid is decreased negative with respect to ground. In cation mode (positive current) at 0 V grid bias, the current measured at the grid is approximately 180 nA and it increases to approximately 200 nA at -80 V bias. This change in current is within the error of the measurement so it cannot be determined that the negative bias on the grid effects electron emission in cation mode. The current measured at the aluminum target plate at 0 V is approximately 380 nA and decreases to approximately 300 nA at -80 V bias on the grid. This change is attributed to the suppression of electron emission from the target surface, but is much smaller than the ~50% drop in cation current measured when biasing the plate positive, results for which are shown in Figure 5a. The emitter and extractor currents in cation mode exhibit no change as the bias on the grid is changed from 0 to -80 V, suggesting that the presence of a grid in front of the target plate may prevent any emitted electrons from travelling upstream to reach the emitter.

In anion mode (negative current) at 0 V grid bias, the current measured at the grid is approximately -200 nA and it becomes less negative, even reaching 0 nA at -30 V grid bias and then becoming positive 30 nA at -80 V grid bias. A positive current measurement suggests the electron emission yield is greater than 1, and more negative electrons are leaving the grid than negative ions arriving at the grid. The current measured at the aluminum target plate at 0 V grid bias is approximately -320 nA and it becomes more negative reaching approximately -400 nA at -80 V grid bias. The extractor current also becomes more negative over this interval from approximately 0 to -70 nA while the emitter current is unchanged. The change in grid, target, and extractor currents in anion mode is attributed to increased electron emission from the negatively biased grid, and emitted electron current arriving at the target plate and the extractor. Figure 7b supports this theory by illustrating the change in currents measured at a negatively biased stainless steel target plate with no grid present. As the bias at the plate becomes more negative from 0 to -60 V, the current measured at the plate in anion mode becomes less negative from -200 nA to 0 nA, similar to the behavior of the stainless steel grid. The currents measured in cation mode are approximately constant as the plate is negatively biased.

V. Analysis and Discussion

A. Ion-Induced Electron Emission Yield

Ion-induced electron emission yield of a material surface is the number of electrons emitted from the surface per ion incident on the surface. Referring to the measured target current of Figure 5, the number of incident ions is the ion current (I_{Ion}) and the number of emitted electrons is the IIEE current (I_{IIEE}), which is the difference between the total current (I_{Total}) and ion current. This relationship for calculating the IIEE yield is equation 2. The calculated IIEE yield as a function of emitter voltage and operating mode for different target materials is shown in Figure 8a.

$$Y_{IIEE} = \frac{|I_{Total} - I_{Ion}|}{I_{Ion}} = \frac{|I_{IIEE}|}{I_{Ion}} \tag{2}$$

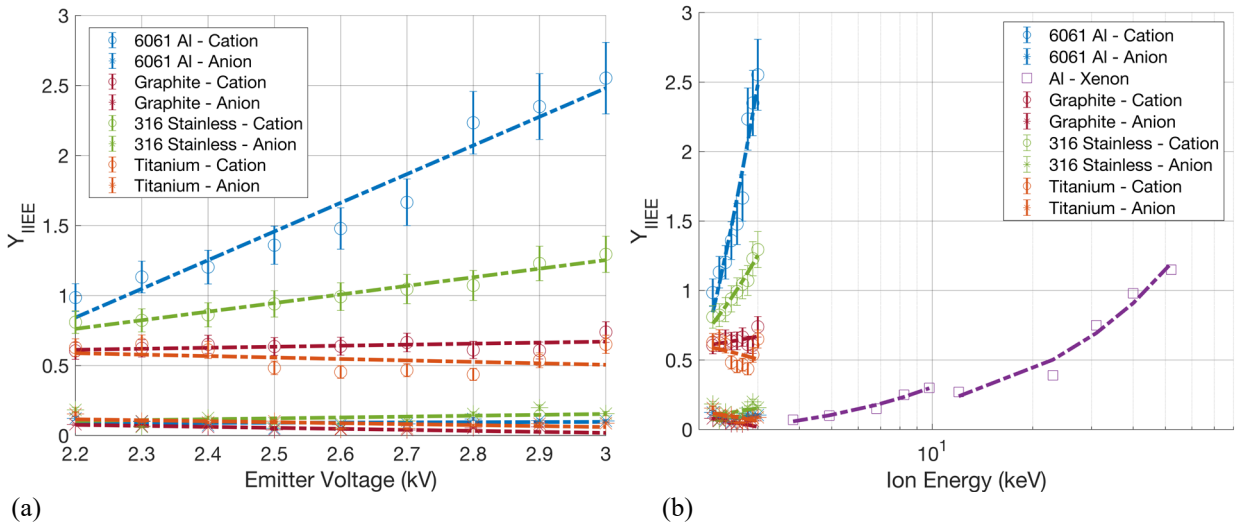

Figure 8: (a) IIEE yields of [EMIM][BF_4] ions impinging on aluminum, graphite, stainless steel, and titanium. (b) Electron emission yields compared to xenon impinging on aluminum.

Figure 8a illustrates the change in IIEE yield for each material in cation and anion mode as the emitter voltage increases from 2.2-3.0 kV. In anion mode, there is no electron emission measured across the entire range of emitter voltages. The calculated yields are < 0.2 for all materials, but the measured changes in current are within the error of the measurement, as discussed earlier. In cation mode, the IIEE yields of carbon graphite and titanium remain constant between 0.5 – 0.7 over this range of emitter voltages. The IIEE yield of stainless steel increases linearly from 0.75 to 1.25 and the yield of aluminum increases from approximately 0.8 to 2.5 making the maximum yield of aluminum in this range 2x higher than stainless steel and 3-4x higher than carbon graphite and titanium.

Figure 8b displays the [EMIM][BF_4] IIEE yield data collected alongside IIEE yields for xenon ions impinging on aluminum [10,11]. The xenon data is over a range of much higher ion energies (4-50 keV) because the range of ion energies (emitter voltages) tested for [EMIM][BF_4] are below the electron emission threshold for xenon impinging on aluminum. The yield for xenon impinging on aluminum reaches 1 at approximately 40 keV whereas [EMIM][BF_4] reaches a yield of 1 at an emitter voltage of 2.3 kV. This comparison illustrates the importance of understanding electron emission to experimental electrospray work.

Recent work by Magnusson et. al. in modelling electron emission from polyatomic ions using the software TRansport of Ions in Matter (TRIM) has been applied to $EMIM^+$ monomer ions [12]. The calculations result in IIEE yields increasing from 0-6 over a range of ion energies from 0.05-15 keV for $EMIM^+$ impinging on stainless steel. In the range from 2-3 keV, the yield increases from approximately 0.4-0.8 compared to measurements here of yields increasing from 0.75-1.25 from 2.2-3.0 kV emitter voltages for stainless steel. Unlike the single species (monomer only), monoenergetic simulations performed by Magnusson et. al., the cation plume used in the experiments described here contains multiple species (monomers, dimers, neutrals) with a distribution in particle/ion energy, as discussed in section IV.A. The lower energy of monomer ions from fragmentation in the plume would suggest the experimental measurements of IIEE yield should be lower than the theoretical calculation. However, the calculation of the IIEE yield by Magnusson et. al. considers the impingement of atoms in the bombarding molecule individually to determine the effect of the bulk molecule. It may be that dimer ions, with more atoms, have a much higher IIEE yield than monomer ions at the same energy, which would explain the higher IIEE yields in the experimental measurements.

B. Electron Emission Suppression Voltage

The voltage at which electron emission is fully suppressed is directly proportional to the energy of electrons emitted from a grounded surface. Electrons leaving the surface with 90 eV of kinetic energy will require a >90 V potential to be drawn back to the target plate. Therefore, the suppression voltage is expected to be equal to the maximum energy of emitted electrons. It is unclear why the suppression voltage is lower when decreasing the potential on the plate than when increasing it, as illustrated by the hysteresis loop in Figure 6a. The suppression voltage as presented here is defined as the target bias voltage, when increasing the target bias voltage from ground, at which the

ion current to the plate changes by <5%. The dependence of suppression voltage on emitter voltage and material is illustrated in Figure 9.

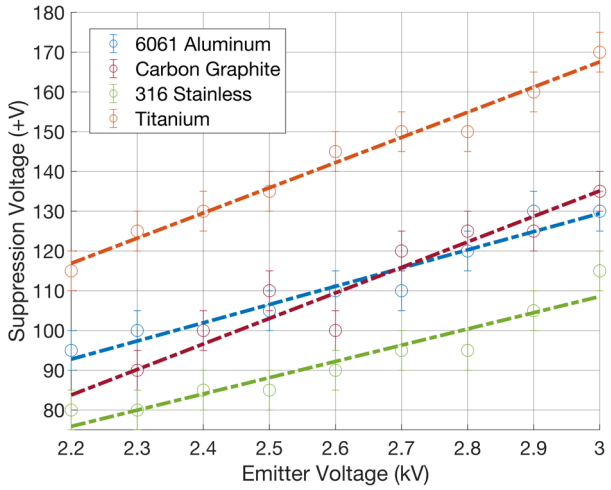

Figure 9: Target plate bias at which electron emission is considered fully suppressed

As illustrated in Figure 9, the suppression voltage for all materials increases over the range of 2.2-3.0 kV emitter voltages. The suppression voltages of titanium and carbon graphite increase by 50 V from 115-165 V and 85-135 V, respectively, while the suppression voltages of aluminum and stainless steel increase by 35 V from 95-130 V and 75-110V, respectively. From these results, it appears that titanium emits electrons at higher energies than the other materials because the suppression voltage for titanium is consistently >20 V higher than all other materials.

C. Current Conservation

Considering the electrical setup of the experiment and assuming current can only travel between emitter, extractor, and target plate, the sum of the extractor and target plate current should be equal to the emitter current. We find this to be true to within ~2.5% for all metallic targets tested (aluminum, titanium, and stainless steel). However, when testing carbon graphite with the same experimental setup the difference between the emitter current and sum of the extractor and target plate current increases to about 15% as illustrated by the ~90 nA gap in emitter and target plate currents in Figure 5b. Further investigation is required to determine what may be causing this discrepancy.

D. Electron Current Returning to Emitter

As discussed in section IV.B, the electrons emitted from the target plate in cation mode appear to be travelling upstream to the emitter, causing the measured emitter current to be higher than the actual ion current emitted. As shown in Figure 2a, the emitter and its electrical contacts are thoroughly wrapped in Kapton tape and all emitter-biased surfaces are therefore shielded and covered. The only path for electrons to reach the emitter potential surfaces is through the hole in the extractor. It may be that space-charge of the cation plume focuses electrons to the extractor hole where they are then focused and guided through the hole by the strong electric field of the emitter-extractor gap. The fraction of electron current returning to the emitter in cation mode is quantified for each test by the ratio of change in emitter current to change in target plate current (change in target plate current is the IIEE current). Specifically, the change in emitter current from no electron suppression (0 V target bias) to full electron suppression is divided by the IIEE current. This ratio is referred to as the returning electron current fraction and is illustrated for all materials in Figure 10.

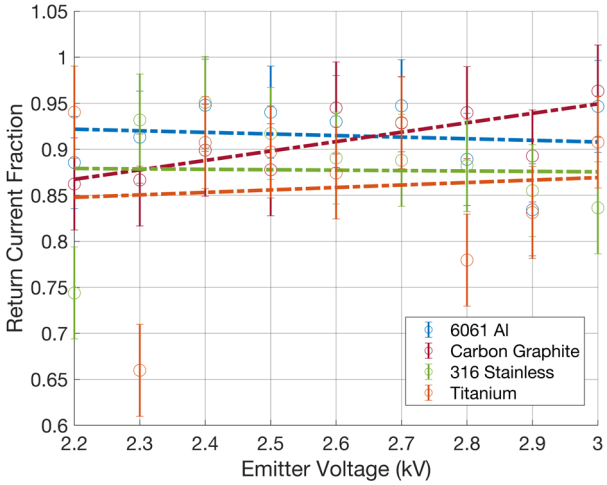

Figure 10: Fraction of electron current returning to the emitter in cation mode

Excluding some outliers, the fraction of electron current returning to the emitter is approximately constant between 85-95% for all metallic materials tested. Carbon graphite may display a slight increasing trend in returning current fraction with increasing emitter voltage, but still within the 85-95% range. This suggests that the material does not have a significant effect on the trajectory of the electrons after leaving the surface in cation mode. Large fractions of electron current returning to the emitter has significant implications for electrospray testing in ground-based facilities. These results suggest that, in addition to electron emission being considered in correcting diagnostic measurements, it must also be considered in correcting the current measured at the emitter or emitter array of a thruster operating in cation mode. It may be possible that electrons emitted from surfaces of diagnostics and from facility walls can be guided towards the extractor hole by space-charge, and then to the emitter by the strong electric field near the extraction region. This would cause the measured thruster/emitter emission current to be higher than the actual ion current leaving the thruster/emitter in cation mode.

VI. Conclusions

IIEE yields for [EMIM][BF_4] electrospray plumes with emitter voltages between 2.2-3.0 kV are between 0.5-2.5 electrons per ion, and electron suppression bias voltage up to +145 V may be required to suppress electron emission from target materials. The yields measured here should be used by experimentalists in electrospray diagnostics to explain and correct anomalous current measurements and be implemented into computational electrospray models to better predict facility effects and the corresponding performance of thrusters in space. Future work should focus on extending these experiments to more space, thruster, and facility relevant target materials (nickel, gold, tungsten, molybdenum, etc.) and electrospray propellants ([EMIM][Im], [EMIM][$EtSO_4$], etc.) as well as a wider range of ion energies. Targeted and focused studies are required to better understand and characterize the IIEE behavior of negatively biased surfaces and electron suppression hysteresis.

Acknowledgments

The authors thank the NASA Early Stage Innovation program, federal award identification number 80NSSC19K0215, for funding the experimental work for this project and Dr. Thomas Liu at NASA Glenn Research Center for his contributions as an advisor for the project. Additionally, the authors thank Dr. Benjamin Prince and Dr. Shawn Miller for hosting Matthew Klosterman at the Air Force Research Laboratory at Kirtland to conduct preliminary externally wetted electrospray experiments.

References

[1] Ma, C., and Ryan, C. "Plume Characterization of a Porous Electrospray Thruster." *The 36th International Electric Propulsion Conference*, 2019, pp. 1–19.

[2] Ma, C., and Ryan, C. N. "The Design and Characterization of a Porous-Emitter Electrospray Thruster (PET-100) for Interplanetary CubeSats." *Proceeding of the 7th Interplanetary CubeSat Workshop*, No. May, 2018, pp. 1–9.

[3] Natisin, M. R., Zamora, H. L., McGehee, W. A., Arnold, N. I., Holley, Z. A., Holmes, M. R., and Eckhardt, D. "Fabrication and Characterization of a Fully Conventionally Machined, High-Performance Porous-Media Electrospray Thruster."

Journal of Micromechanics and Microengineering, Vol. 30, No. 11, 2020, p. 115021. doi:10.1088/1361-6439/abb8c3.
[4] Petro, E. M., Bruno, A. R., Lozano, P. C., Perna, L. E., and Freeman, D. S. "Characterization of the Tile Electrospray Emitters." *AIAA Propulsion and Energy 2020 Forum*, 2020, pp. 1–13. doi:10.2514/6.2020-3612.
[5] Mier-Hicks, F., and Lozano, P. C. "Spacecraft-Charging Characteristics Induced by the Operation of Electrospray Thrusters." *Journal of Propulsion and Power*, Vol. 33, No. 2, 2017, pp. 456–467. doi:10.2514/1.B36292.
[6] Ma, C. (University of S. *Design and Characterization of Electrospray Thrusters with High Emission Density*. University of Southampton, 2020.
[7] Coles, T. M., Fedkiwf, T. P., and Lozanot, P. C. Investigating Ion Fragmentation in Electrospray Thruster Beams. 2012.
[8] Lozano, P., and Martínez-Sánchez, M. "Ionic Liquid Ion Sources: Characterization of Externally Wetted Emitters." *Journal of Colloid and Interface Science*, Vol. 282, No. 2, 2005, pp. 415–421. doi:10.1016/j.jcis.2004.08.132.
[9] Lozano, P., and Martínez-Sánchez, M. "On the Dynamic Response of Externally Wetted Ionic Liquid Ion Sources." *Journal of Physics D: Applied Physics*, Vol. 38, No. 14, 2005, pp. 2371–2377. doi:10.1088/0022-3727/38/14/011.
[10] Alonso, E. V., Baragiola, R. A., Ferrn, J., Jakas, M. M., and Oliva-Florio, A. "Z1 Dependence of Ion-Induced Electron Emission from Aluminum." *Physical Review B*, Vol. 22, No. 1, 1980, pp. 80–87. doi:10.1103/PhysRevB.22.80.
[11] Svensson, B., Holmén, G., and Burén, A. "Angular Dependence of the Ion-Induced Secondary-Electron Yield from Solids." *Physical Review B*, Vol. 24, No. 7, 1981, pp. 3749–3755. doi:10.1103/PhysRevB.24.3749.
[12] Magnusson, J. M., Collins, A. L., and Wirz, R. E. "Polyatomic Ion-Induced Electron Emission (Iiee) in Electrospray Thrusters." *Aerospace*, Vol. 7, No. 11, 2020, pp. 1–21. doi:10.3390/aerospace7110153.